8-2023

Predicting Postfire Sediment Yields of Small Steep Catchments Using Airborne Lidar Differencing

James J. Guilinger

Efi Foufoula-Georgiou

Andrew B. Gray

James T. Randerson

Padhraic Smyth

See next page for additional authors

Authors

James J. Guilinger, Efi Foufoula-Georgiou, Andrew B. Gray, James T. Randerson, Padhraic Smyth, Nicolas C. Barth, and Michael L. Goulden

Geophysical Research Letters

RESEARCH LETTER
10.1029/2023GL104626

Predicting Postfire Sediment Yields of Small Steep Catchments Using Airborne Lidar Differencing

James J. Guilinger[1,2], Efi Foufoula-Georgiou[2,3], Andrew B. Gray[4], James T. Randerson[2,3], Padhraic Smyth[5], Nicolas C. Barth[6], and Michael L. Goulden[3]

[1]Department of Applied Environmental Science, California State University, Seaside, CA, USA, [2]Department of Civil and Environmental Engineering, University of California, Irvine, Irvine, CA, USA, [3]Department of Earth System Science, University of California, Irvine, Irvine, CA, USA, [4]Department of Environmental Sciences, University of California, Riverside, Riverside, CA, USA, [5]Department of Computer Sciences, University of California, Irvine, Irvine, CA, USA, [6]Department of Earth and Planetary Sciences, University of California, Riverside, Riverside, CA, USA

Key Points:

- Postfire dry and wet sediment transport were quantified with lidar and dominant controls were identified using random forest regression
- Slope and sediment supply, including dry ravel, were the strongest controls on initial sediment yield by debris flows and floods
- Continued sediment bulking occurred from soil erosion and patchy mass wasting later in the wet season as channels became supply limited

Supporting Information:

Supporting Information may be found in the online version of this article.

Correspondence to:

J. J. Guilinger,
jguilinger@csumb.edu

Citation:

Guilinger, J. J., Foufoula-Georgiou, E., Gray, A. B., Randerson, J. T., Smyth, P., Barth, N. C., & Goulden, M. L. (2023). Predicting postfire sediment yields of small steep catchments using airborne lidar differencing. *Geophysical Research Letters*, *50*, e2023GL104626. https://doi.org/10.1029/2023GL104626

Received 19 MAY 2023
Accepted 13 AUG 2023

Abstract

Predicting sediment yield from recently burned areas remains a challenge but is important for hazard and resource management as wildfire impacts increase. Here we use lidar-based monitoring of two fires in southern California, USA to study the movement of sediment during pre-rainfall periods and postfire periods of flooding and debris flows over multiple storm events. Using a data-driven approach, we examine the relative importance of terrain, vegetation, burn severity, and rainfall amounts through time on sediment yield. We show that incipient fire-activated dry sediment loading and pre-fire colluvium were rapidly flushed out by debris flows and floods but continued erosion occurred later in the season from soil erosion and, in ~9% of catchments, from shallow landslides. Based on these observations, we develop random forest regression models to predict dry ravel and incipient runoff-driven sediment yield applicable to small steep headwater catchments in southern California.

Plain Language Summary

Wildfire makes watersheds more susceptible to hazardous flash flooding and debris flows, yet characterization and prediction of these hazards remains limited. In this study, we used repeat airborne laser mapping to quantify the movement of sediment in steep burn areas during initial dry periods and subsequent erosion from runoff events. Based on these observations, we developed two predictive models: one to predict the filling of channels with sediment prior to rainfall and a second one to predict erosion by debris flows and floods during initial storm events, which showed improvement over another commonly used model. After initial runoff events, much of the available sediment in channels was transported downstream, however small landslides and extensive erosion of soils across the landscape continued to supply sediment to floods and debris flows, in line with studies elsewhere showing continued debris flow activity despite reduced sediment in channels. Our study demonstrates that airborne laser mapping together with data-driven modeling offer opportunities to increase predictive ability of post-fire erosion and such approaches should be further explored in regions such as northern California, where fire is expanding and models of post-fire erosion need to be tested and refined.

1. Introduction

Wildfire is a major biophysical disturbance to mountainous systems worldwide. Fire fundamentally alters soil properties and reduces vegetation cover, both of which can dramatically increase watershed runoff and erosional responses to rainfall for months to years following fire (Shakesby & Doerr, 2006). A legacy of fire exclusion practices and ongoing changes to climate have exacerbated the intensity and extent of wildfire in many mountainous regions (Westerling et al., 2006), with climate-induced trends expected to amplify over the 21st century (Williams et al., 2019). Additionally, climate change is increasing peak rainfall intensities (e.g., AghaKouchak et al., 2018; Lenderink et al., 2017), which increases the likelihood of postfire flooding and debris flows (Kean & Staley, 2021; Oakley, 2021). Debris flows are destructive geophysical flows composed of water, sediment, and organic material such as wood and ash (Gabet & Sternberg, 2008; Iverson, 1997) that can impair downstream water resources, destroy infrastructure, and threaten lives in wildland-urban interfaces. The focus of this study is on southern California, where the 2018 Montecito debris flows claimed 23 lives and led to damage totaling >0.5 billion USD (Kean et al., 2019).

Although recent work has advanced empirical and physically-based models for postfire hazard scenarios (e.g., Hoch et al., 2021; Raymond et al., 2020; Staley et al., 2017), the complex interaction of topography, geology, rainfall forcing, and burn severity on post-wildfire hazards necessitates a greater understanding of the controls on post-wildfire sediment yield. The most commonly used postfire debris-flow (PFDF) hazard framework is the combined USGS models for PFDF probability (Staley et al., 2017) and volume (Gartner et al., 2014). These models collectively rely on data from semiarid western US, primarily from southern California PFDFs, and use slope, burn severity, rainfall intensity, and soil erodibility estimates as predictors for PFDF flow occurrence and magnitude. Yet, recent work has shown that model performance may degrade in very steep watersheds, even in the same region for which the model was developed (DiBiase & Lamb, 2020). In very steep (>32°), bedrock-dominated, semi-arid terrain, a dominant postfire geomorphic process is dry ravel. Dry ravel describes a general process of the movement of particles downslope by rolling, sliding, and bouncing that becomes exacerbated following the combustion of soil stabilizing vegetation (e.g., Florsheim et al., 1991; Gabet, 2003). Dry ravel contributes to debris flow susceptibility by filling up channels with fine-grained material that can be more easily mobilized by runoff (DiBiase & Lamb, 2020; Palucis et al., 2021). Conversely, in terrain with thicker and more continuous soil cover, monitoring has shown that a large share of debris flow material comes from shallow soil erosion across hillslopes in magnitudes that correspond well to burn severity and rainfall intensity (e.g., Guilinger et al., 2020; Rengers et al., 2021; Staley et al., 2014). The complexity of many simultaneously operating runoff and erosion processes poses a challenge for the prediction of PFDF magnitude. Unraveling the dominant controls on postfire sediment yield would help advance a further mechanistic understanding of postfire sediment flux processes in steep terrain.

Airborne lidar elevation datasets are becoming increasingly ubiquitous across the western US (USGS, 2023). With a larger extent of high-resolution elevation data available, we now have the ability to rapidly map erosion and sediment redistribution in mountainous catchments impacted by recent fire across much broader areas (DiBiase & Lamb, 2020; Morell et al., 2021; Rengers et al., 2021). Building off this expanding data platform, we use multitemporal remote sensing data to quantify both dry and wet sediment transfer processes in the 2018 Holy Fire in southern California, USA and dry sediment transfer processes in the 2020 Apple Fire. For the 2018 Holy Fire, we quantified sediment yield from channel networks using a set of 6 repeat airborne lidar scanning (ALS) datasets over ~31 km^2 of burn area with $n = 566$ headwater catchments (Figure 1a) spanning both initial dry weather sediment loading of channels and subsequent PFDFs and flood events during a wetter than average rainy season following fire (Figure 1c). The Apple Fire data set ($n = 157$ watersheds, area = ~7 km^2) covered a period of dry ravel channel loading and was used as an independent data set for model testing. Using a co-located network of rain gauges, satellite reflectance products, and other widely available environmental variables, we asked the following questions: (a) What is the relative importance of various environmental controls on post-fire dry sediment loading and post-fire runoff and PFDF sediment yields? (b) How does erosion vary through time as sediment is continually eroded from headwater streams in the first wet season prior to significant vegetation recovery? We employed a data-driven approach to train models with random forest regression (RFR) to assess variable importance and predict dry ravel loading and subsequent runoff-driven sediment yield.

2. Study Area and Methods

2.1. Study Areas

The primary study area was the 2018 Holy Fire in southern California, USA. The wildfire burned ~94 km^2 through steep (~15 to > 45°) terrain dominated by chaparral vegetation and underlain by two dominant lithologies: Jurassic metasedimentary units composed of highly fractured argillites and quartzites and Cretaceous granitic bedrock (Morton & Miller, 2006). Initial postfire assessments by state and federal agencies (Schwartz & Stempniewicz, 2018; USGS, 2018) and field observations (Guilinger et al., 2020; Wilder et al., 2021) noted landscape conditions known to increase PFDF susceptibility such as enhanced soil-water repellency and loading of channel networks with loose material through dry ravel processes. We also used dry ravel data from the 2020 Apple Fire (Figure 2) as a validation data set. The fire burned ~135 km^2 of chaparral-dominated steep terrain underlain by Precambrian granitic rocks and gneisses in the San Bernardino Mountain foothills of southern California. Most of the area assessed was burned at moderate or high severity (56%) and there was pervasive dry ravel loading of headwater channels (Figure 2), generating similar concern of PFDF hazards in foothill communities within and downstream of the burned hillslopes (USGS, 2020).

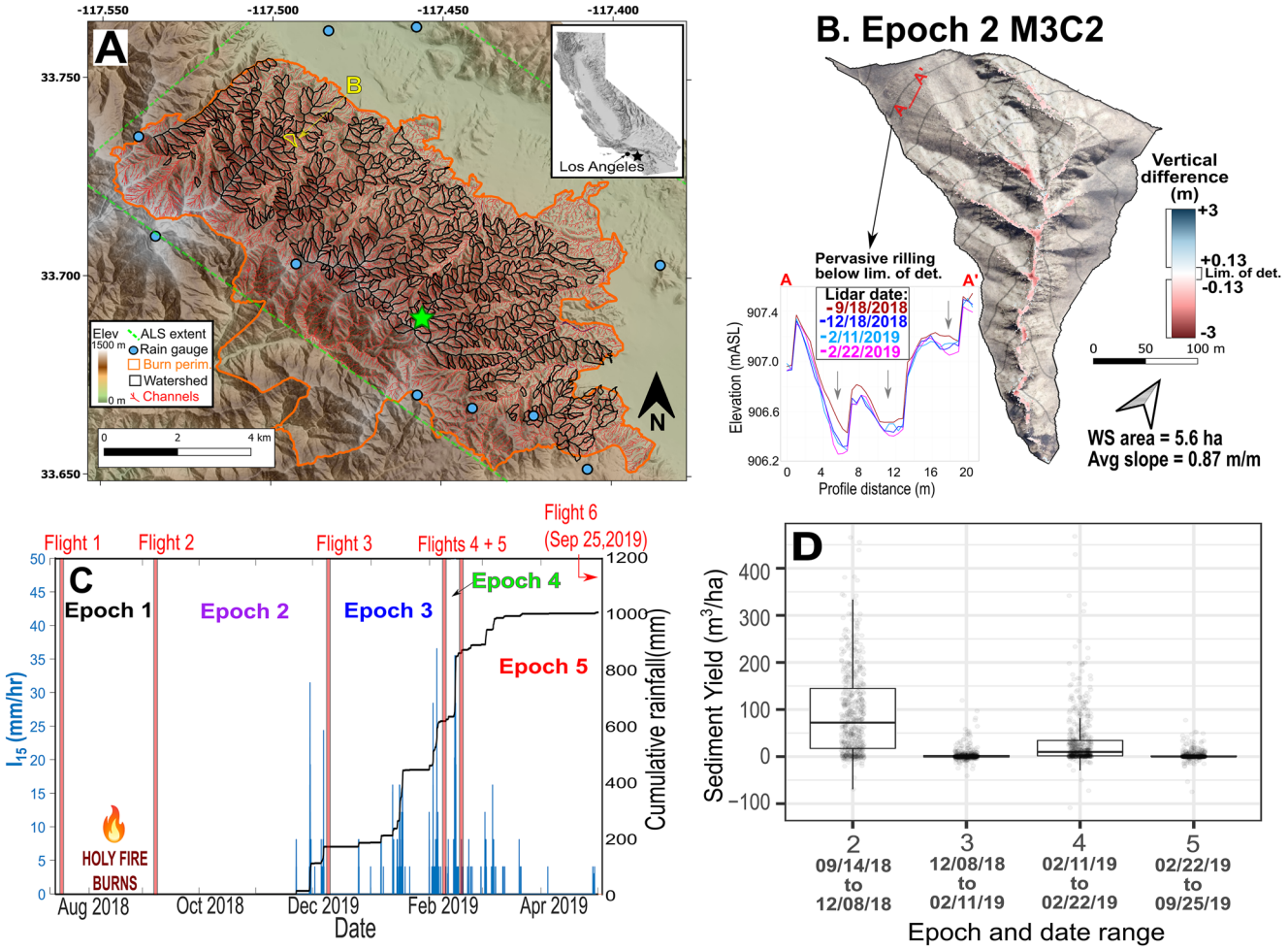

Figure 1. (a) Colored shaded relief map showing the 566 sub-catchments (black outlines) used in this study across the Holy Fire burn area (orange outline). Green dashed outline shows the extent of repeat airborne lidar scanning (ALS) data. Blue circles show the network of tipping-bucket rain gauges ($n = 11$) and green star corresponds to the gauge data shown in (c). (b) Example of ALS differencing (M3C2 method of Lague et al., 2013) surface differencing map. Red corresponds to erosion and blue corresponds to deposition. Inset shows cross section (A to A') of ALS DEMs that shows the formation and growth of rills below the limit of change detection. (c) Time series of 15-min rainfall intensity (I_{15}) and cumulative rainfall for Horsethief Canyon gauge (green star in (a)) and ALS epochs. Epoch 1 was a period of zero rainfall and captured sediment loading by dry ravel. (d) Boxplots and point jitters showing distribution of sediment yields due to runoff-driven erosion during Epochs 2–5 in the Holy Fire (negative yields = in-channel storage).

2.2. Geospatial Analysis

We used ALS datasets from pre-fire acquisitions by the US Geological Survey, postfire flights from Riverside County Flood Control and Water Conservation District (4 in the Holy Fire and 1 in the Apple Fire), and a flight from an NCALM seed award. Because these datasets were initially collected in separate coordinate systems, they were coarsely aligned through datum transformations in LAStools and finely registered using rigid-body iterative-closest point registration in CloudCompare. We used the multiscale model-to-model cloud comparison (M3C2) algorithm (Lague et al., 2013) to estimate signed differences between successive point clouds in the vertical direction, filtered these changes by estimated detection limits (~0.12 m), and estimated sediment yield from the net difference of erosion and deposition volumes normalized to catchment area (see Text S1 in Supporting Information S1 for more information).

2.3. Random Forest Regression Model and Predictive Assessment

We used random forest regression (RFR) to develop predictive models of dry ravel loading of channels in Epoch 1 (referred to as *RFR1*) and sediment yield due to runoff processes for Epoch 2 (referred to as *RFR2*); see Figure 1c

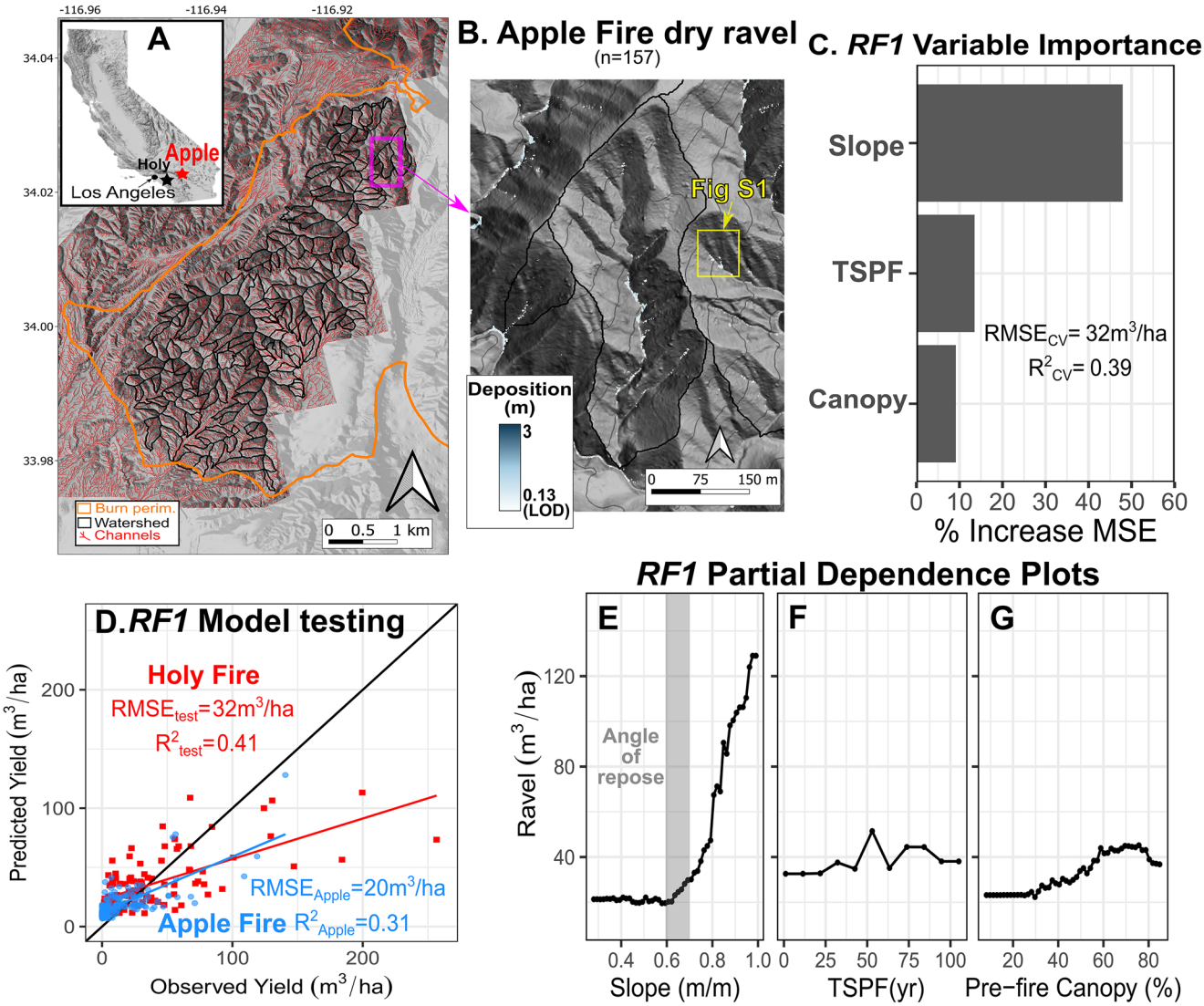

Figure 2. (a) Map showing the 157 watersheds within the Apple Fire burn area (burned August 2020 with pre-fire USGS flight in 2018 and postfire flight in August 2020). (b) Zoomed in example of catchments experiencing dry ravel loading verified by Google Earth imagery (see Figure S1 in Supporting Information S1). Note that LOD = limit of detection. (c) Variable importance plot for dry ravel predictors of *RFR1* with cross validation performance metrics (R^2 and RMSE). Note that RMSE = root mean squared error. (d) Model testing on both Holy Fire test holdout (red) and independent Apple Fire ravel data set (blue). (e–g) Partial dependence plots for three variables used in the final model (note: TSPF = time since previous fire). Slope had the greatest marginal effect and sharp increase in ravel activity corresponded to typical angle of repose values for soils in the region (Lamb et al., 2011).

for the definition of rainfall Epochs. RFR was chosen over parametric methods because along with other machine learning models, it does not impose any functional relationships between variables, where complex nonlinear associations may exist between hydrogeomorphic variables in rainfall-runoff scenarios (Moody et al., 2013). RFR is a modeling framework which is an extension of decision tree regression, where decision tree splits are selected to minimize mean square error, but model robustness is improved by building an ensemble of regression trees where individual trees are built through bootstrap samples of data points and random subsets of predictor variables (Breiman, 2001). Training of RFRs to predict dry ravel loading in Epoch 1 (*RFR1*) and runoff-generated sediment yield in Epoch 2 (*RFR2*) was performed in R programming language using the package *caret* using a scheme of cross-validation of training data and model testing on held out from model training (see Text S1 in Supporting Information S1 for more information).

For *RFR1*, we chose the following predictors for ravel loading: watershed average slope, time since previous fire, and percent canopy cover from pre-fire lidar (Table S1 in Supporting Information S1), allowing this model

to be applicable to future fires in very steep catchments of southern California and similar fire-prone areas with accurate inventories of fire history and lidar coverage. For *RFR2* we chose the following predictors for sediment yield: watershed average slope, ravel loading, time since previous fire, burn severity (from difference normalized burn ratio), burn area, cumulative precipitation over survey epoch, peak 15-min rainfall intensity, normalized vegetation difference index, and geology (Table S1 in Supporting Information S1). The model with the lowest RMSE was selected and predictive performance was assessed using the 20% held out data from the Holy Fire for both models and spatially independent Apple Fire data in *RFR1*. Additionally, we compared *RFR2* to model outputs from the Gartner et al. (2014) debris volume model as an assessment of predictions. For both RFR models, partial dependence plots (Friedman, 2001) were made for certain predictors (see Text S1 in Supporting Information S1). These plots show the average effect that a predictor has on dry ravel (*RFR1*) or sediment yield (*RFR2*). Because of widespread sediment supply limitations in channels and valley bottoms, we could not build robust RFR models for Epochs 3–5, therefore we used *RFR2* to predict sediment yield for a large atmospheric river storm event during Epoch 4 to assess changes in sediment yield patterns later on in the season, which is described in Section 3.4.

3. Results and Discussion

3.1. Holy Fire Dry and Wet Erosion Periods

During Epoch 1, we resolved volumetric loading of dry ravel across a large fraction of headwater channels situated below steep burned hillslopes (Figures S1 and S2 in Supporting Information S1). Rainfall rates at or slightly above regional thresholds for PFDF risk (>20–24 mm/hr for 15-min durations) occurred across the burn scar on 29 November and 5 December 2018, resulting in the most extensive erosion during the study period (Figure 1b). Epochs 3 and 4 included storm events with rainfall intensities near or exceeding those of Epoch 2. During Epoch 3, very little channel sediment yield was detected by ALS; a majority (~72%) of catchments instead experienced minor amounts of channel infilling (negative yield values), which was ultimately sourced from hillslope erosion below the limit of detection of ALS differencing (Figure 1b inset). In Epoch 4, a strong atmospheric river made landfall over the study area, resulting in the highest sustained rainfall intensities and elevated sediment yield relative to Epoch 3, although still less than Epoch 2. The remainder of the study period in Epoch 5 featured the lowest rainfall intensities and very little sediment yield detected from ALS differencing.

3.2. Predicting Dry Ravel Loading of Channels

During initial model development of random forest regression *(RFR1)* for dry ravel prediction, we found little evidence of a relationship between dry ravel and burn severity. Variable importance of *RFR1* shows that dry ravel response is dominated by slope, with time since previous fire and pre-wildfire canopy having approximately equal, but lesser importance (Figure 2c). Cross-validation showed that model performance was similar between the Holy Fire and Apple Fire, with slightly decreased performance for the latter (Figures 2c and 2d). In model testing, ravel response was overpredicted for most catchments and underpredicted for catchments with more extreme responses in both fires (Figure 2d). Despite somewhat modest predictive power and bias for the independent test datasets, *RFR1* did appear to capture the relative risk of dry ravel loading and identified the most hazardous catchments accurately.

Consistent with previous work on dry ravel dynamics, slope exerted a strong first-order control on dry ravel loading (Gabet, 2003). *RFR1* partial plots (Figure 2e) show a strong marginal effect of slope in the form of an exponential increase in ravel loading beyond the range of angle of repose for most soil materials (0.6–0.7, ~30–35°). The marginal effects of time since previous fire and pre-fire canopy density were much more modest but were both positive (2F-G). This dependence of ravel yield on fire history and vegetation density is consistent with previous studies which found that dry ravel supply in steep landscapes (>32°) is dependent on soil production between wildfires and plant stem density (DiBiase & Lamb, 2013; Lamb et al., 2011).

3.3. Prediction of Incipient Erosion

Random forest regression of runoff-mediated sediment yield during Epoch 2 (*RFR2*) revealed that geomorphic variables such as watershed slope, pre-runoff ravel, and time since previous fire were dominant variables in

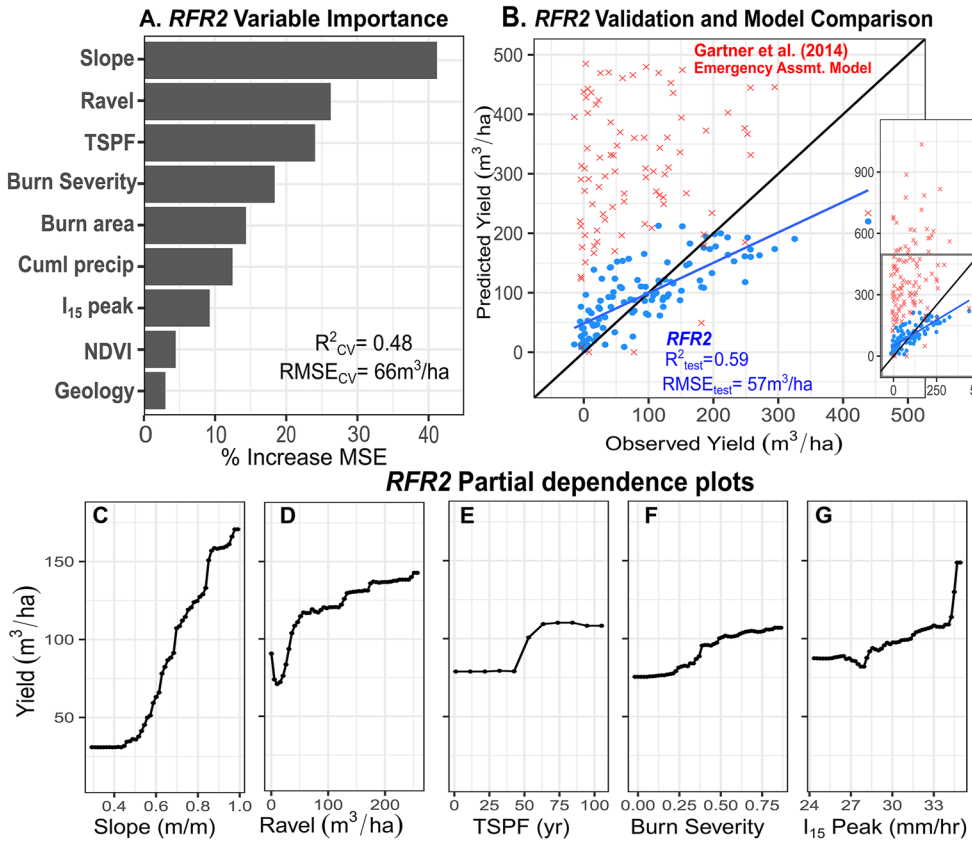

Figure 3. (a) Variable importance plots for Random Forest regression of Epoch 2 (*RFR2*) and cross validation performance metrics (R^2 and RMSE). Note that I_{15} peak = peak 15 min rainfall intensity, TSPF = time since previous fire, cuml precip = total accumulated precipitation, and NDVI = normalized difference vegetation index. (b) Evaluation of the *RFR2* against held-out testing data (blue points) with best fit line showing that the model on average moderately overpredicts at smaller sediment yield values and underpredicts at larger yield values, with similar R^2 and RMSE to cross-validation. Red crosses show predictions for the same catchments using the Gartner et al. (2014) Emergency Assessment Model, which results in poor performance and overall overprediction. Inset shows same plot but includes the full range of predicted values. (c) Partial dependence plots showing the marginal relationship between selected parameters (the top 4 predictors in plot A and I_{15}).

predicting sediment yield in response to the initial two rainfall events in Epoch 2 (Figure 3). Burn severity and burn area were the next most important predictors, followed by rainfall intensity, cumulative precipitation, and NDVI, with little influence from geology. *RFR2* obtained moderate predictive power (R^2_{test} = 0.59), yielding similar predictive power to the existing Gartner et al. (2014) model (see Figure S3 in Supporting Information S1). Using our test data, *RFR2* performed better than the volume model of Gartner et al. (2014), which tended to over-predict yields relative to our model (Figure 3b). The overestimation of the Gartner volume at small drainage areas, such as those investigated here (<0.3 km^2), has also been found in another study by Rengers et al. (2021). Part of this may stem from this model being trained on volume data from a wider range of catchment areas (0.01–27.9 km^2). The importance of dry ravel and fire history in *RFR2* indicates that including these sediment supply terms may improve model predictions for small fire-impacted catchments where debris flows initiate in southern California (e.g., Palucis et al., 2021).

3.4. Seasonal Regime Shift

We observed a reduction of sediment yield from headwater channel networks as estimated by ALS (Figure 1) and ground-based observations of channel downcutting to bedrock following initial events of Epoch 2 (Figure S4 in Supporting Information S1), supported by field observations of scour to bedrock floors of headwater valleys and channels. We were unable to obtain robust RF models for later epochs due to these supply limitations. Instead,

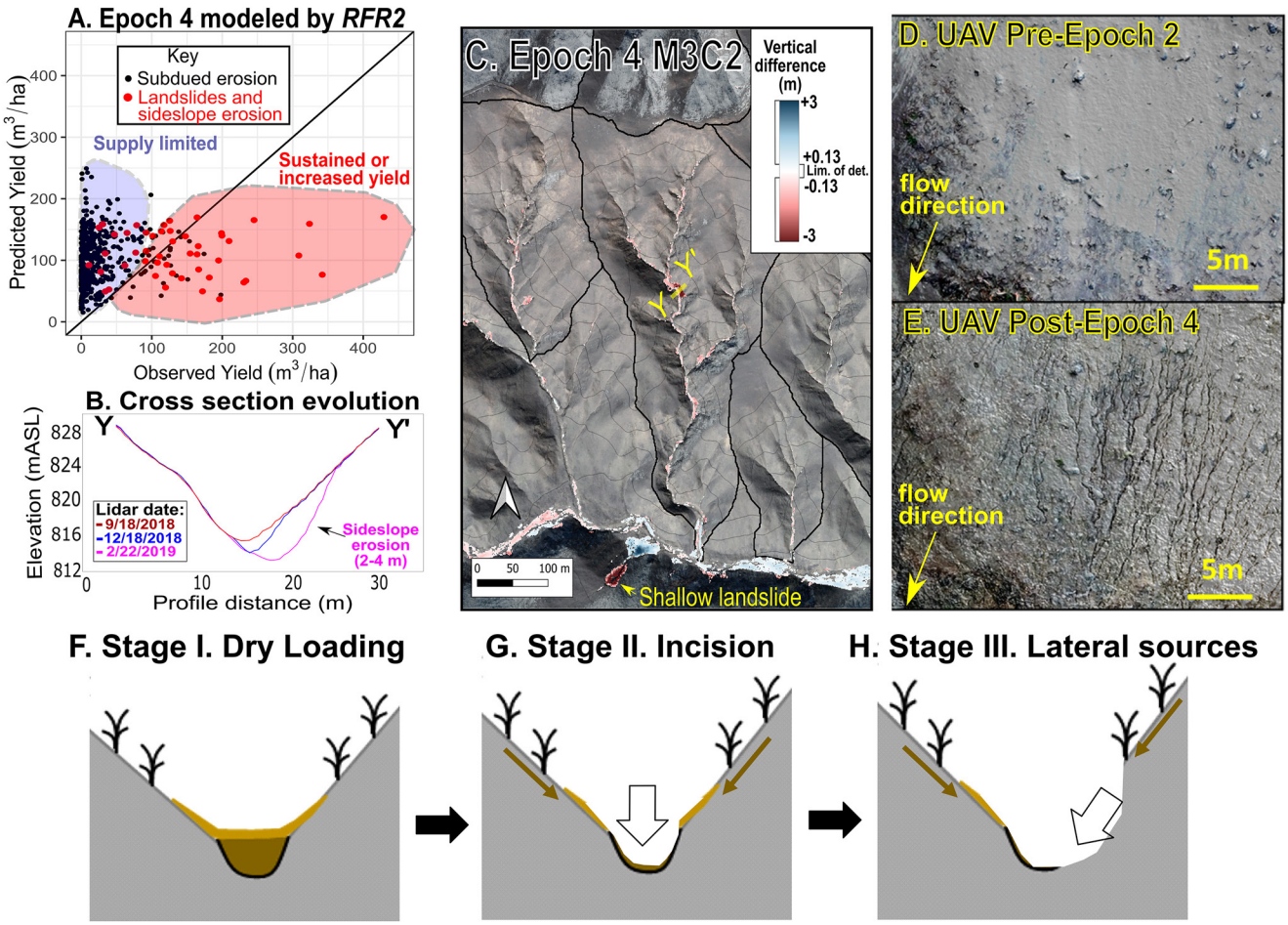

Figure 4. (a) Predicted sediment for Epoch 4 yield using *RFR2* versus observed sediment yield. General regions showing supply-limited catchments versus catchments with significant hillslope erosion from slope failures or channel-adjacent erosion. (b) Cross-section detailing time evolution of a second order headwater channel with pre-runoff surface, initial sediment evacuation during Epoch 2 (December 2018) and side-slope failure (2–4 m in depth) (c) Holy Fire Epoch 4 erosion map showing example slope failures, with Y to Y' transect corresponding to cross-section. (d) UAS-derived orthoimages prior to wet season showing bare hillslopes and (e) following Epoch 4 showing significant rill erosion covering the same extent. (f) Illustration of valley cross section showing Stage I of conceptual model of dry ravel loading. (g) Stage II illustrating channel incision by initial PFDFs and floods. (h) Stage III illustrating lateral sources of sediment via sideslope erosion along channels. Brown arrows indicate contributions of soil erosion in Stages II and III.

RFR2 was used to model Epoch 4 response and compared to observed sediment yield (Figure 4a) in order to assess if controls on sediment yield were similar between the two Epochs. Poor fit between *RFR2* predictions and observed yields indicated that there is an overall shift in the hydrogeomorphic controls on sediment yield with one cluster of points indicating supply limitations and the other dominated by catchments with clear evidence of shallow soil failures that primarily occurred along channel sideslopes (Figures 4b and 4c).

The general decrease in sediment availability within channels and patchy spatial distribution of slope failures and near-channel instability indicates that controls on mass wasting may become more important over time, although specific catchment-scale relationships are not obvious (Figure S5 in Supporting Information S1). Preliminary support for this hypothesis includes field observations of late-season saturation of unstable soil-mantled hillslopes (evidence of saturated conditions from Guilinger et al., 2020) and significant erosion along over-steepened channel margins (Figures 4b and 4c). Despite generally decreased sediment yield from processes detectable with ALS (primarily channel erosion), hydrologic monitoring during Epoch 4 showed evidence of continued PFDFs and sediment-laden flooding in steep tributary streams (Guilinger et al., 2020). As shown in both ALS data (cross-section inset of Figure 1b) and UAS surveys (Figures 4d and 4e), erosion through shallow hillslope processes such as rilling and sheetflow were evident throughout the study, including Epoch 4. This implies that hillslope erosion persisted as a source of sediment for later season PFDFs and floods even though channels

became rapidly sediment supply-limited following Epoch 2, as has been found in other studies of recent burn areas (<1 year post-fire) subject to repeated rainfall (e.g., Santi & MacAulay, 2019; Staley et al., 2014; Tang et al., 2019).

3.5. Study Limitations and Uncertainties

Uncertainty exists in many input variables, which could explain some of the unexplained variance for both RFR1 and RFR2. A co-located study of hillslope erosion using terrestrial lidar found that channelized erosion that is resolvable with ALS accounted for >50% of sediment yield during Epoch 2, however shallow hillslope erosion played an important role in overall yield and its relative role increased through time as channels became supply-limited during Epochs 3–5 (Guilinger et al., 2020). Therefore, ALS provides minimum estimates for total watershed yields. The presence of smaller ravel cones in imagery not detected through change analysis (Figures S1 and S2 in Supporting Information S1) also indicates some underprediction for these values as well. Additionally, internal geomorphic controls such as fine-scale temporal variations in surface grain size properties that vary over event to seasonal timescales are important sources of variability in predicting sediment yield (Saletti et al., 2015), but are typically difficult or impossible to measure (Kim et al., 2016). These processes are potentially important as previous work has found that PFDF initiation thresholds can be impacted by shifts in grain size caused by size-selective transport processes (Hoch et al., 2021).

An additional limitation of this study is that we train models on data from a single burn scar. For example, total rainfall accumulations and 15-min intensities were relatively uniform (Figure S5 in Supporting Information S1) across the study area in Epoch 2, and through all epochs 15-min intensities were near predicted thresholds for PFDF initiation based on the USGS probability model (Staley et al., 2017). This may explain the greater relative importance of geomorphic and sediment supply variables as compared to rainfall. This contrasts with previous work which included a wider array of hydrologic response data varied over many rainfall intensities in order to determine specific rainfall thresholds for PFDF response (Staley et al., 2017) and magnitude (Gartner et al., 2014).

4. Concluding Remarks

Based on our work and other studies in the region (e.g., DiBiase & Lamb, 2020; Rengers et al., 2021; Schmidt et al., 2011; Staley et al., 2014; Tang et al., 2019), we propose a conceptual multistage model of sediment redistribution and yield from burned steep headwater catchments in southern California prior to revegetation (Figures 4f–4h). In Stage I, dry ravel fills in hollows and channels that prime the channel for Stage II where sufficient rainfall scours channels down to bedrock, limiting the amount of hollow and valley-bottom sediments. Stage III is marked by a lateral erosion phase where mass wasting of channel margins and thicker soils later in the season and persistent soil erosion continues to supply sediment to floods and PFDFs.

Although additional data from more burn areas could be used to test and refine the models presented here, our study demonstrated improvements relative to a commonly-used model for post-fire sediment yield for small (<0.2 km^2), steep (>30°) headwater catchments where dry ravel is a common process, making it applicable to many regions of southern California prone to PFDFs. With an increase in available lidar data as topographic baselines, similar hydrologic and geomorphic change detection studies should be employed in mountainous regions experiencing large increases in fire where predictive models need to be tested and refined.

Data Availability Statement

2018 USGS airborne lidar data used in this study can be obtained from NOAA Digital Coast: https://coast.noaa.gov/dataviewer/. 2019 OpenTopography lidar data can be obtained at: https://portal.opentopography.org/datasetMetadata?otCollectionID=OT.072020.6340.1. Reflectance based remote sensing data can be obtained from: https://earthengine.google.com/. Additional data and R machine learning scripts are located here: https://osf.io/tds49/?view_only=90361e2e14434b3b9f5fd8d1154ff048.

Acknowledgments
This research was supported by the NSF TRIPODS+X program (Grant DMS-1839336), Center for Ecosystem Climate Solutions (funding from the California Strategic Growth Council Climate Change Research Program), USDA NIFA Hatch Project CA-R-ENS-5120-H, USDA Multi-State Project W4188, and NASA Global Precipitation Measurement Program (Grant 80NSSC22K0597). We greatly appreciate Riverside County Flood Control and Water Conservation District, US Geological Survey, and National Center for Airborne Laser Mapping (award ID: OT.072020.6340.1, hosted on OpenTopography) for acquiring ALS used in this study. We appreciate discussions with Janine Baijnath-Rodino, Lawrence Vulis, Hongbo Ma, and Phong Le about this work. We also thank editor Valeriy Ivanov and two anonymous reviewers whose comments helped improved this manuscript.

References

AghaKouchak, A., Ragno, E., Love, C., & Moftakhari, H. (2018). Projected changes in Californias precipitation intensity-duration-frequency curves. In *California's fourth climate change assessment*. California Energy Commission. Retrieved from https://www.energy.ca.gov/sites/default/files/2019-11/CCCA4-CEC-2018-005_ADA.pdf

Breiman, L. (2001). Random forests. *Machine Learning*, *45*(1), 5–32. https://doi.org/10.1023/A:1010933404324

DiBiase, R. A., & Lamb, M. P. (2013). Vegetation and wildfire controls on sediment yield in bedrock landscapes. *Geophysical Research Letters*, *40*(6), 1093–1097. https://doi.org/10.1002/grl.50277

DiBiase, R. A., & Lamb, M. P. (2020). Dry sediment loading of headwater channels fuels post-wildfire debris flows in bedrock landscapes. *Geology*, *48*(2), 189–193. https://doi.org/10.1130/G46847.1

Florsheim, J. L., Keller, E. A., & Best, D. W. (1991). Fluvial sediment transport in response to moderate storm flows following chaparral wildfire, Ventura County, southern California. *Geological Society of America Bulletin*, *103*(4), 504–511. https://doi.org/10.1130/00167606(1991)103<0504:FSTIRT>2.3.CO;2

Friedman, J. H. (2001). Greedy function approximation: A gradient boosting machine. *Annals of Statistics*, *29*(5), 1189–1232. https://doi.org/10.1214/aos/1013203451

Gabet, E. J. (2003). Sediment transport by dry ravel. *Journal of Geophysical Research*, *108*(B1), 1–8. https://doi.org/10.1029/2001JB001686

Gabet, E. J., & Sternberg, P. (2008). The effects of vegetative ash on infiltration capacity, sediment transport, and the generation of progressively bulked debris flows. *Geomorphology*, *101*(4), 666–673. https://doi.org/10.1016/j.geomorph.2008.03.005

Gartner, J. E., Cannon, S. H., & Santi, P. M. (2014). Empirical models for predicting volumes of sediment deposited by debris flows and sediment-laden floods in the transverse ranges of southern California. *Engineering Geology*, *176*, 45–56. https://doi.org/10.1016/j.enggeo.2014.04.008

Guilinger, J. J., Gray, A. B., Barth, N. C., & Fong, B. T. (2020). The evolution of sediment sources over a sequence of postfire sediment-laden flows revealed through repeat high-resolution change detection. *Journal of Geophysical Research: Earth Surface*, *125*(10), 1–23. https://doi.org/10.1029/2020JF005527

Hoch, O. J., McGuire, L. A., Youberg, A. M., & Rengers, F. K. (2021). Hydrogeomorphic recovery and temporal changes in rainfall thresholds for debris flows following wildfire. *Journal of Geophysical Research: Earth Surface*, *126*(12), e2021JF006374. https://doi.org/10.1029/2021jf006374

Iverson, R. M. (1997). The physics of debris flows. *Reviews of Geophysics*, *35*(97), 245–296. https://doi.org/10.1029/97RG00426

Kean, J. W., & Staley, D. M. (2021). Forecasting the frequency and magnitude of postfire debris flows across southern California. *Earth's Future*, *9*(3), 1–19. https://doi.org/10.1029/2020EF001735

Kean, J. W., Staley, D. M., Lancaster, J. T., Rengers, F. K., Swanson, B. J., Coe, J. A., et al. (2019). Inundation, flow dynamics, and damage in the 9 January 2018 Montecito debris-flow event, California, USA: Opportunities and challenges for post-wildfire risk assessment. *Geosphere*, *15*(4), 1140–1163. https://doi.org/10.1130/GES02048.1

Kim, J., Ivanov, V. Y., & Fatichi, S. (2016). Soil erosion assessment—Mind the gap. *Geophysical Research Letters*, *43*(24), 12–446. https://doi.org/10.1002/2016GL071480

Lague, D., Brodu, N., Leroux, J., Rennes, G., Rennes, U., & Beaulieu, C. (2013). Accurate 3D comparison of complex topography with terrestrial laser scanner: Application to the Rangitikei canyon (NZ). *ISPRS Journal of Photogrammetry and Remote Sensing*, *82*, 10–26. https://doi.org/10.1016/j.isprsjprs.2013.04.009

Lamb, M. P., Scheingross, J. S., Amidon, W. H., Swanson, E., & Limaye, A. (2011). A model for fireinduced sediment yield by dry ravel in steep landscapes. *Journal of Geophysical Research*, *116*(3), 1–13. https://doi.org/10.1029/2010JF001878

Lenderink, G., Barbero, R., Loriaux, J. M., & Fowler, H. J. (2017). Super-Clausius–Clapeyron scaling of extreme hourly convective precipitation and its relation to large-scale atmospheric conditions. *Journal of Climate*, *30*(15), 6037–6052. https://doi.org/10.1175/JCLI-D-16-0808.1

Moody, J. A., Shakesby, R. A., Robichaud, P. R., Cannon, S. H., & Martin, D. A. (2013). Current research issues related to post-wildfire runoff and erosion processes. *Earth-Science Reviews*, *122*, 10–37. https://doi.org/10.1016/j.earscirev.2013.03.004

Morell, K. D., Alessio, P., Dunne, T., & Keller, E. (2021). Sediment recruitment and redistribution in mountain channel networks by post-wildfire debris flows. *Geophysical Research Letters*, *48*(24), e2021GL095549. https://doi.org/10.1029/2021GL095549

Morton, D. M., & Miller, F. K. (2006). *Geologic map of the San Bernardino and Santa Ana 30′ X 60′ Quadrangles, California*. US Geological Survey.

Oakley, N. S. (2021). A warming climate adds complexity to post-fire hydrologic hazard planning. *Earth's Future*, *9*(7). https://doi.org/10.1029/2021ef002149

Palucis, M. C., Ulizio, T. P., & Lamb, M. P. (2021). Debris flow initiation from ravel-filled channel bed failure following wildfire in a bedrock landscape with limited sediment supply. *GSA Bulletin*, *133*(9–10), 1–18. https://doi.org/10.1130/b35822.1

Raymond, C. A., McGuire, L. A., Youberg, A. M., Staley, D. M., & Kean, J. W. (2020). Thresholds for post-wildfire debris flows: Insights from the Pinal fire, Arizona, USA. *Earth Surface Processes and Landforms*, *45*(6), 1349–1360. https://doi.org/10.1002/esp.4805

Rengers, F. K., McGuire, L. A., Kean, J. W., Staley, D. M., Dobre, M., Robichaud, P. R., & Swetnam, T. (2021). Movement of sediment through a burned landscape: Sediment volume observations and model comparisons in the San Gabriel Mountains, California, USA. *Journal of Geophysical Research: Earth Surface*, *126*(7), 1–25. https://doi.org/10.1029/2020jf006053

Saletti, M., Molnar, P., Zimmermann, A., Hassan, M. A., & Church, M. (2015). Temporal variability and memory in sediment transport in an experimental step-pool channel. *Water Resources Research*, *51*(11), 9325–9337. https://doi.org/10.1002/2015WR016929

Santi, P. M., & MacAulay, B. (2019). Rainfall intensity limitation and sediment supply independence of post-wildfire debris flows in the western U.S. In *Debris-flow hazards mitigation: Mechanics, monitoring, modeling, and assessment—Proceedings of the 7th international conference on debris-flow hazards mitigation, (2005)* (pp. 539–547).

Schmidt, K. M., Hanshaw, M. N., Howle, J. F., Kean, J. W., Staley, D. M., Stock, J. D., & Bawden, G. W. (2011). Hydrologic Conditions and Terrestrial Laser Scanning of Postfire Debris Flows in the San Gabriel Mountains, CA, U.S.A. Debris-Flow Hazards Mitigation. *Mechanics, Prediction, and Assessment*, 583–593. https://doi.org/10.4408/IJEGE.2011-03.B-064

Schwartz, J. W., & Stempniewicz, T. (2018). *Burned area emergency response (BAER) assessment—Geologic hazards for Holy Fire*. United States National Forest. Retrieved from https://www.fs.usda.gov/Internet/FSE_DOCUMENTS/fseprd594862.pdf

Shakesby, R. A., & Doerr, S. H. (2006). Wildfire as a hydrological and geomorphological agent. *Earth-Science Reviews*, *74*(3–4), 269–307. https://doi.org/10.1016/j.earscirev.2005.10.006

Staley, D. M., Negri, J. A., Kean, J. W., Laber, J. L., Tillery, A. C., & Youberg, A. M. (2017). Prediction of spatially explicit rainfall intensity–duration thresholds for postfire debris-flow generation in the western United States. *Geomorphology*, *278*, 149–162. https://doi.org/10.1016/j.geomorph.2016.10.019

Staley, D. M., Wasklewicz, T. A., & Kean, J. W. (2014). Characterizing the primary material sources and dominant erosional processes for postfire debris-flow initiation in a headwater basin using multi-temporal terrestrial laser scanning data. *Geomorphology*, *214*, 324–338. https://doi.org/10.1016/j.geomorph.2014.02.015

Tang, H., McGuire, L. A., Rengers, F. K., Kean, J. W., Staley, D. M., & Smith, J. B. (2019). Evolution of debris-flow initiation mechanisms and sediment sources during a sequence of postwildfire rainstorms. *Journal of Geophysical Research: Earth Surface*, *124*(6), 1572–1595. https://doi.org/10.1029/2018JF004837

US Geological Survey. (2018). Holy fire postfire debris flow preliminary hazard assessment. *USGS Landslide Hazards Program*. Retrieved from https://landslides.usgs.gov/hazards/postfire_debrisflow/detail.php?objectid=205

US Geological Survey. (2020). El dorado and apple postfire debris flow preliminary hazard assessment. *USGS Landslide Hazards Program*. Retrieved from https://landslides.usgs.gov/hazards/postfire_debrisflow/detail.php?objectid=297

US Geological Survey. (2023). 3D elevation program. Retrieved from https://www.usgs.gov/3d-elevation-program

Westerling, A. L., Hidalgo, H. G., Cayan, D. R., & Swetnam, T. W. (2006). Warming and earlier spring increase Western U.S. forest wildfire activity. *Science*, *313*(5789), 940–943. https://doi.org/10.1126/science.1128834

Wilder, B. A., Lancaster, J. T., Cafferata, P. H., Coe, D. B. R., Swanson, B. J., Lindsay, D. N., et al. (2021). An analytical solution for rapidly predicting postfire peak streamflow for small watersheds in southern California. *Hydrological Processes*, *35*(1), 1–14. https://doi.org/10.1002/hyp.13976

Williams, A. P., Abatzoglou, J. T., Gershunov, A., Guzman-Morales, J., Bishop, D. A., Balch, J. K., & Lettenmaier, D. P. (2019). Observed impacts of anthropogenic climate change on wildfire in California. *Earth's Future*, *7*(8), 892–910. https://doi.org/10.1029/2019EF001210

References From the Supporting Information

Schwanghart, W., & Scherler, D. (2014). TopoToolbox 2—MATLAB-based software for topographic analysis and modeling in Earth surface sciences. *Earth Surface Dynamics*, *2*, 1–7. https://doi.org/10.5194/esurf-21-2014